Author/s:
Canver, MC;Tripathi, P;Bullen, MJ;Olshansky, M;Kumar, Y;Wong, LH;Turner, SJ;Lessard, S;Pinello, L;Orkin, SH;Das, PP

Title:
A saturating mutagenesis CRISPR-cas9–mediated functional genomic screen identifies cis- And trans-regulatory elements of oct4 in murine ESCs

Date:
2020-11-20

Citation:
Canver, M. C., Tripathi, P., Bullen, M. J., Olshansky, M., Kumar, Y., Wong, L. H., Turner, S. J., Lessard, S., Pinello, L., Orkin, S. H. & Das, P. P. (2020). A saturating mutagenesis CRISPR-cas9–mediated functional genomic screen identifies cis- And trans-regulatory elements of oct4 in murine ESCs. Journal of Biological Chemistry, 295 (47), pp.15797-15809. https://doi.org/10.1074/jbc.RA120.013772.

Persistent Link:
https://hdl.handle.net/11343/290389

A saturating mutagenesis CRISPR-Cas9–mediated functional genomic screen identifies *cis*- and *trans*-regulatory elements of *Oct4* in murine ESCs

Received for publication, April 6, 2020, and in revised form, September 15, 2020 Published, Papers in Press, September 29, 2020, DOI 10.1074/jbc.RA120.013772

Matthew C. Canver[1,‡], Pratibha Tripathi[2,3,‡], Michael J. Bullen[2,3,‡], Moshe Olshansky[4,5], Yogesh Kumar[2,3], Lee H. Wong[6], Stephen J. Turner[4,7], Samuel Lessard[8,9], Luca Pinello[10], Stuart H. Orkin[1,11,*], and Partha Pratim Das[2,3,*]

From the [1]Division of Hematology/Oncology, Boston Children's Hospital and Department of Pediatric Oncology, Dana–Farber Cancer Institute (DFCI), Harvard Stem Cell Institute, Harvard Medical School, Boston, Massachusetts, USA, the [2]Department of Anatomy and Developmental Biology, Monash University, Clayton, Victoria, Australia, the [3]Development and Stem Cells Program, the [4]Department of Microbiology, and the [6]Department of Biochemistry and Molecular Biology, Cancer Program, Monash Biomedicine Discovery Institute, Monash University, Clayton, Victoria, Australia, [5]Computational Biology and Bioinformatics, Baker Heart and Diabetes Institute, Melbourne, Victoria, Australia, the [7]Department of Microbiology and Immunology, University of Melbourne, Parkville, Victoria, Australia, the [8]Research Center, Montreal Heart Institute, Montréal, Quebec, Canada, the [9]Department of Medicine, Faculty of Medicine, Université de Montréal, Montréal, Quebec, Canada, the [10]Molecular Pathology and Cancer Center, Massachusetts General Hospital and Harvard Medical School, Boston, Massachusetts, USA, and the [11]Howard Hughes Medical Institute, Boston, Massachusetts, USA

Edited by John M. Denu

Regulatory elements (REs) consist of enhancers and promoters that occupy a significant portion of the noncoding genome and control gene expression programs either in *cis* or in *trans*. Putative REs have been identified largely based on their regulatory features (co-occupancy of ESC-specific transcription factors, enhancer histone marks, and DNase hypersensitivity) in mouse embryonic stem cells (mESCs). However, less has been established regarding their regulatory functions in their native context. We deployed *cis*- and *trans*-regulatory elements scanning through saturating mutagenesis and sequencing (ctSCAN-SMS) to target elements within the ~12-kb *cis*-region (*cis*-REs; CREs) of the *Oct4* gene locus, as well as genome-wide 2,613 high-confidence *trans*-REs (TREs), in mESCs. ctSCAN-SMS identified 10 CREs and 12 TREs as novel candidate REs of the *Oct4* gene in mESCs. Furthermore, deletions of these candidate REs confirmed that the majority of the REs are functionally active, and CREs are more active than TREs in controlling *Oct4* gene expression. A subset of active CREs and TREs physically interact with the *Oct4* promoter to varying degrees; specifically, a greater number of active CREs, compared with active TREs, physically interact with the *Oct4* promoter. Moreover, comparative genomics analysis reveals that a greater number of active CREs than active TREs are evolutionarily conserved between mice and primates, including humans. Taken together, our study demonstrates the reliability and robustness of ctSCAN-SMS screening to identify critical REs and investigate their roles in the regulation of transcriptional output of a target gene (in this case *Oct4*) in their native context.

Large-scale genomic studies reveal that ~80% of the human genome may be involved in gene regulation, whereas only ~2% of the genome encodes proteins (1). The functional noncoding genome can be broadly divided into regulatory elements (REs) and regions that encode noncoding RNAs (1, 2). Furthermore, REs can be subdivided into *cis*-REs (CREs) and *trans*-REs (TREs), based on their position relative to their target gene(s). CREs are present proximally or distally relative to their target gene on the same chromosome, whereas TREs are located distally relative to their target gene on different chromosomes (3, 4). Putative REs have been identified using various methods, including transcription factor binding, enhancer histone marks, DNA accessibility (open chromatin regions), enhancer-promoter interactions, and gene expression (1, 5–10). REs are usually enriched with sequence variants that are associated with diverse human traits and diseases (11–13). In addition, REs play crucial roles in evolutionary turnover and divergence (14–17).

Initial efforts systematically evaluated RE functions using reporter assays on a massive scale (18, 19); however, such approaches fail to interrogate RE functions within their native genomic contexts. Advances in CRISPR-Cas9–mediated genome editing technology (20, 21) have transformed analysis of protein-coding genes (22, 23) as well as REs *in situ* in chromatin. A few high-throughput CRISPR-Cas9–mediated functional genetic screens were performed to characterize CREs in mammalian cells (24–29). Prior screens to identify functional CREs were focused on either targeting putative CREs of gene(s) of interest (gene-centric) or targeting putative CREs bound by selected TFs (TF-centric). Nevertheless, identification of functional TREs presents a challenge that has attracted less attention.

Here, we deployed genome-wide *cis*- and *trans*-regulatory elements scanning through saturating mutagenesis and sequencing (ctSCAN-SMS) in mouse embryonic stem cells (mESCs) to

This article contains supporting information.

‡These authors contributed equally to this work.
*For correspondence: Stuart H. Orkin, stuart_orkin@dfci.harvard.edu; Partha Pratim Das, partha.das@monash.edu.
Present address for Samuel Lessard: Rare Blood Disorders, Sanofi, Waltham, Massachusetts, USA.

identify critical CREs and TREs of the *Pou5f1*/*Oct4* gene (a master pluripotency regulator of mESCs). We uncovered new functionally active CREs and TREs and how they regulate *Pou5f1*/*Oct4* gene expression in mESCs.

Results

Design of a saturating CRISPR-Cas9 pooled library for ctSCAN-SMS

In mESCs, several putative REs, including 8,563 enhancers (ENs) and 231 superenhancers (SEs) have been identified based on co-occupancy of ESC-specific TFs (OCT4, NANOG, SOX2, KLF4, and ESRRB), mediators (MED1), enhancer histone marks (H3K4me1 and H3K27ac), and DNase I hypersensitivity (30). SEs contain multiple ENs; SEs are also more densely co-occupied with TFs, enhancer histone marks, and chromatin regulators, as compared with ENs, and associate with greater transcriptional output (30). We undertook a high-throughput CRISPR-Cas9–mediated genome-editing approach to comprehensively target putative REs in mESCs. First, we generated a genome-wide map of open chromatin regions using ATAC-Seq in mESCs, as ATAC-Seq identifies most EN REs (10). ATAC-Seq peaks were then overlaid within all putative ENs (8,563) and SEs (231) to designate "high-confidence" REs (2,613) (Fig. 1*a*, Fig. S1*a*, and Table S1). As these REs are distributed genome-wide and on different chromosomes relative to the *Oct4* gene locus (in *trans*), we termed these REs TREs. All possible single guide RNAs (sgRNAs) (20 nt) were designed (within the TREs for tilling) upstream of the *Streptococcus pyogenes* Cas9 NGG-protospacer-adjacent motif (PAM) sequences to target the high-confidence 2,613 TREs (Fig. 1*a*, Fig. S1*a*, and Tables S1 and S2). This analysis yielded 70,480 sgRNAs with a median gap of 5 bp between adjacent genomic cleavages (Fig. 1, *c* and *d*). Likewise, 1,827 sgRNAs were designed at the surrounding ~12-kb (−10 to +2 kb of the TSS of the *Oct4*) region of the mouse *Oct4* gene locus to dissect the CREs of *Oct4* (Fig. 1, *b* and *c*). In addition, the library included 2,000 nontargeting (NT) sgRNAs as negative controls, 119 sgRNAs targeting GFP (of the *Oct4*-GFP reporter that used for the screen), and 150 sgRNAs targeting coding sequence of mESC-TFs as positive controls (Fig. 1*c*). In total, the RE CRISPR-Cas9 pooled library contained 74,576 sgRNAs (Fig. 1*c*). These sgRNAs were synthesized, pooled, and cloned into a lentiviral vector for deep sequencing. The deep sequencing of the pooled library confirmed the presence of >95% sgRNAs that target TREs and >99% sgRNAs that target CREs and control sgRNAs (Fig. S1 (*b–f*) and Table S2).

Candidate CREs and TREs of the Oct4 gene identified by ctSCAN-SMS

The pooled library was transduced into an *Oct4*-GFP reporter mESC line, which constitutively expresses Cas9 (31–33). The *Oct4*-GFP reporter was used as a "readout" for the screen to measure the reduction in GFP levels upon perturbation of any targeted RE regions by their corresponding sgRNAs. Lentiviral transduction of the pooled library was performed at low multiplicity (MOI) to ensure that each cell contained predominantly one sgRNA (Fig. S2*a*). After puromycin drug selection (because sgRNA constructs carry the puromycin drug resistance gene), "GFP-low" cells were sorted using FACS (Fig. S2, *a* and *b*). As a control, cells were collected before FACS (the "pre-sort" sample). Genomic DNA was isolated from both "GFP-low" and "pre-sort" cell populations, and next-generation sequencing was employed to enumerate the sgRNAs in each population (Fig. S2*a*). The screen was performed in triplicate.

We calculated an "enrichment score" of each sgRNA by comparing its frequency (presence) in GFP-low over pre-sort cells. Enrichment scores were determined based on the two best replicates (Table S2). The highest and lowest enrichment scores obtained from GFP-targeting sgRNAs (mean $\log_2$FC 4.87, $p <$ 0.0001) and NT sgRNAs (mean $\log_2$FC 0.44, $p < 0.0001$) indicated that the screen was technically successful (Fig. 2*a* and 3*a*). We ranked all sgRNAs based on their enrichment scores (Table S2) and analyzed their off-target scores (ranging between 0 and 100) (34) (Figs. S3*a* and S4*a* and Table S2). A higher off-target score signifies fewer off-targets of an sgRNA. We found that the majority of the evaluated sgRNAs (87.6% sgRNAs for CREs and 84.5% sgRNAs for TREs) had off-target scores >10 (Table S2); these sgRNAs are statistically significant based on the hidden Markov model (HMM) analysis (Fig. S3*a*).

To identify candidate CREs of the *Oct4*, we considered all HMM sgRNAs with off-target scores >10 and mapped them within the ~12-kb surrounding region (−10 to +2 kb of TSS) of the *Oct4* gene locus. This yielded 16 candidate CREs (numbered 1–16), based on the mean enrichment score (mean $\log_2$FC) of sgRNAs per CRE. Each of the candidate CREs had a mean $\log_2$FC > 0.5 (range of mean $\log_2$FC 0.93–3.95), with $p <$ 0.0001, which was higher than the mean enrichment score of NT sgRNAs (mean $\log_2$FC 0.44, with $p < 0.0001$) (Fig. 2, *a* and *b*). Among 16 CREs, CREs 10 and 12 have been recognized previously as distal and proximal enhancers, respectively (31); CREs 13–16 were present within the promoter region of *Oct4* (±2 kb of TSS) (31). The remaining 10 CREs were newly identified candidate CREs of the *Oct4* gene (Fig. 2, *a* and *b*). Of note, CRE 12 displayed a relatively lower mean enrichment score ($\log_2$FC 0.77, $p < 0.0001$) compared with other candidate CREs, because the original *Oct4*-GFP reporter lacks a portion of CRE 12 (33). Nonetheless, we included CRE 12 for further validation.

To classify the candidate TREs, we applied a statistically relevant HMM analysis to the sgRNA enrichment scores (35), which initially identified 263 candidate TREs. Furthermore, we applied stringent criteria to select candidate TREs for validation, as follows: (i) TREs must have HMM sgRNAs with off-target scores >10 (Fig. 3*a* and Fig. S4*a*); (ii) TREs must possess at least four sgRNAs with mean $\log_2$FC >0.5 (range of mean $\log_2$FC 0.86–2.52), with $p < 0.0001$ (Fig. 3*b*); (iii) TREs must co-occupy with ESC-TFs (OCT4, NANOG, and SOX2) and enhancer histone marks (H3K27ac and H3K4me1) (Fig. 3*c* and Fig. S4*b*); and (iv) they must contain "dynamic" open chromatin regions (*i.e.* "open" chromatin regions present in the undifferentiated state (0 h) that gradually become "closed" with differentiation (24 and 96 h) of mESCs) (Fig. 3*d* and Fig. S4*c*). Based on these criteria, we selected 12 candidate TREs of the *Oct4* gene (Fig. 3, *a* and *b*).

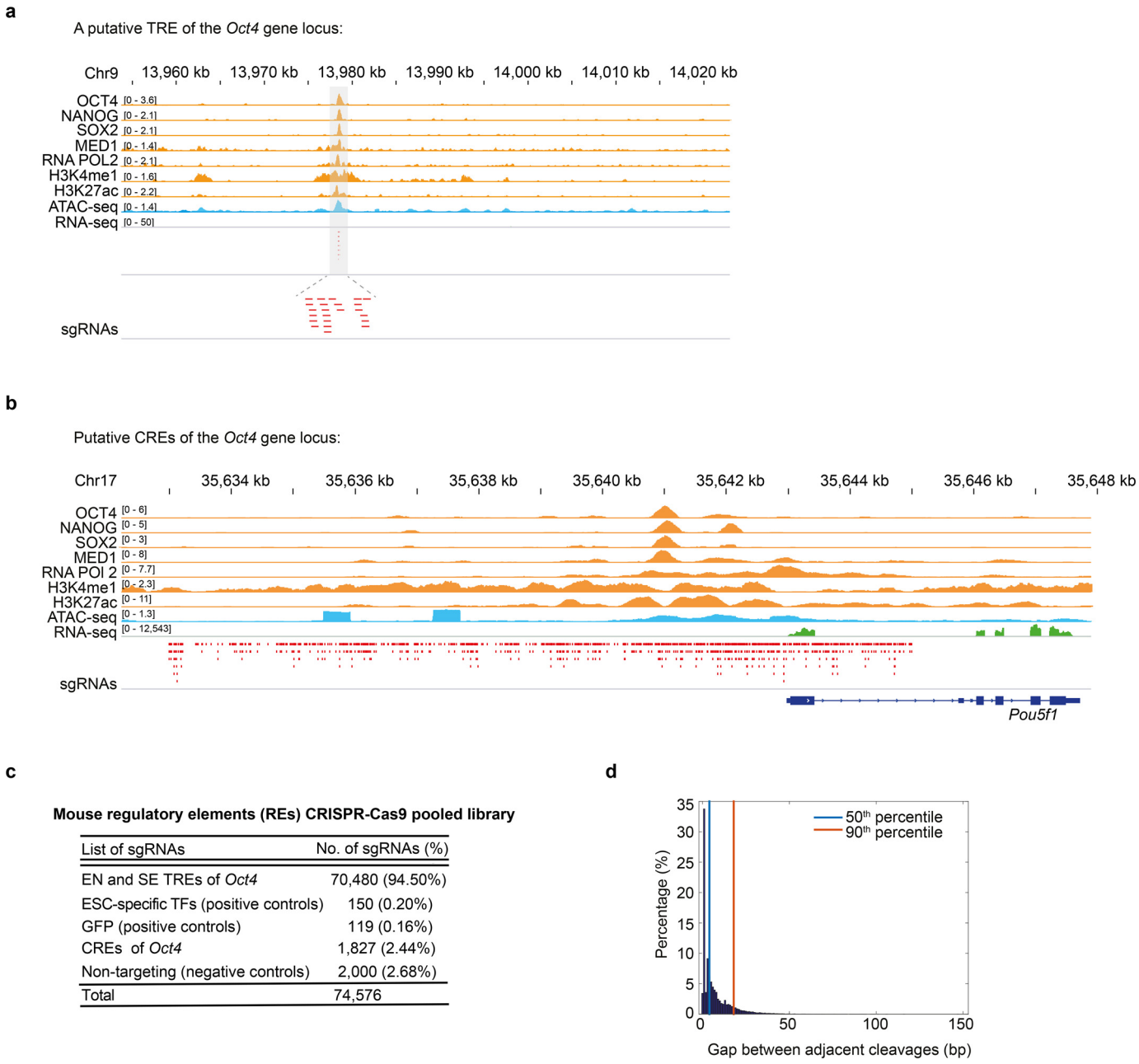

c

Mouse regulatory elements (REs) CRISPR-Cas9 pooled library

List of sgRNAs	No. of sgRNAs (%)
EN and SE TREs of *Oct4*	70,480 (94.50%)
ESC-specific TFs (positive controls)	150 (0.20%)
GFP (positive controls)	119 (0.16%)
CREs of *Oct4*	1,827 (2.44%)
Non-targeting (negative controls)	2,000 (2.68%)
Total	74,576

Figure 1. Design of a saturating CRISPR-Cas9 pooled library for ctSCAN-SMS. *a*, genomic tracks show co-occupancy of ESC-TFs (OCT4, NANOG, and SOX2), mediator (MED1), enhancer histone marks (H3K27ac and H3K4me1), and RNA Pol2 at a putative TRE of the *Oct4* gene locus in mESCs. The ATAC-Seq track represents open chromatin regions and ENs; the RNA-Seq track represents gene expression. The *highlighted region* displays a putative TRE. All possible sgRNAs (shown with *red dashed lines*) were designed upstream of PAM sequences (NGG) within the putative TRE. *b*, genomic tracks illustrate co-occupancy of ESC-TFs (OCT4, NANOG, and SOX2), mediator (MED1), enhancer histone marks (H3K27ac and H3K4me1), and RNA Pol2 at putative CREs of the *Oct4* gene locus in mESCs. The ATAC-Seq track characterizes open chromatin regions and enhancers; the RNA-Seq track represents gene expression. sgRNAs (shown with *red dashed lines*) tilled upstream of PAM sequences (NGG) at the ~12-kb surrounding region (*cis* region) of the *Oct4* locus. *c*, mouse RE CRISPR-Cas9 pooled library distribution. *d*, gaps between adjacent genomic cleavages of NGG PAM sgRNAs targeting CREs and TREs of the *Oct4*.

Dissection of functionally active CREs and TREs of the Oct4 gene

We selected a total of 33 REs, including 20 CREs (16 candidate CREs and 4 control CREs (CREs with no significant enrichment scores of sgRNAs)) and 13 TREs (12 candidate TREs and one control TRE (with no significant enrichment scores of sgRNAs)) of the *Oct4* gene locus for validation using WT mESCs. "Paired" sgRNAs (5′ and 3′ sgRNAs) tagged with mCherry were used to target both of the flanking ends of each selected candidate RE to create a deletion. Following transfection of paired sgRNAs-mCherry into the WT mESCs, mCherry-positive cells were sorted to measure the endogenous Oct4 mRNA expression and to confirm the genomic deletions of CREs/TREs (Figs. 2*f* and 3*e*, Figs. S3*d* and S4*e*, and Table S3). We observed a significant reduction in Oct4 expression to different extents upon deletions of CREs 1, 3, 5, 7, 10, 12, and 13–16 (of 16 candidate CREs) (Fig. 2*f*). Deletions of newly identified CREs 1, 3, 5, and 7 showed a greater reduction in Oct4

a

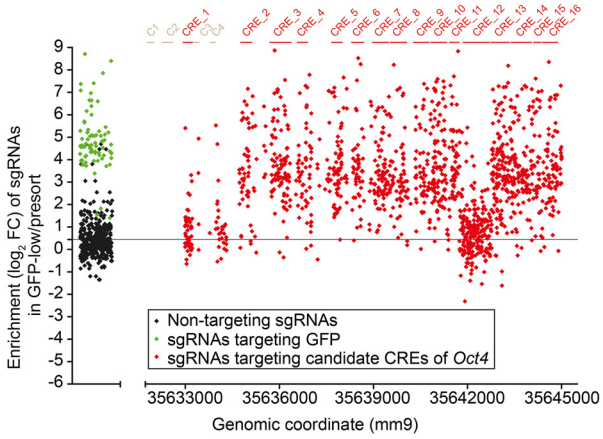

b

List of candidate CREs of the *Oct4* gene

Based on mean enrichment scores (mean log2FC) of sgRNAs (in GFP-low/pre-sort) per CRE. Candidate CREs have mean log2FC >0.5, P-values <0.0001. All the HMM sgRNAs per CRE have off-target score >10.

Candidate CREs	Genomic locations of REs (mm9) (enriched sgRNAs)	Length (bp)	No. of sgRNAs
CRE_1	chr17:35,632,944-35,633,217	273	51
CRE_2	chr17:35,634,773-35,635,108	335	40
CRE_3	chr17:35,635,706-35,636,370	664	98
CRE_4	chr17:35,636,568-35,636,884	316	35
CRE_5	chr17:35,637,687-35,637,998	311	53
CRE_6	chr17:35,638,316-35,638,663	347	45
CRE_7	chr17:35,638,981-35,639,479	498	73
CRE_8	chr17:35,639,516-35,640,048	532	60
CRE_9	chr17:35,640,274-35,640,811	537	56
CRE_10	chr17:35,640,811-35,641,342	531	97
CRE_11	chr17:35,641,411-35,641,715	304	50
CRE_12	chr17:35,641,862-35,642,696	834	187
CRE_13	chr17:35,642,726-35,643,342	616	140
CRE_14	chr17:35,643,343-35,644,057	714	113
CRE_15	chr17:35,644,097-35,644,345	248	35
CRE_16	chr17:35,644,380-35,644,880	500	70
Control CRE_1 (C1)	chr17:35,631,818-35,631,951	133	0
Control CRE_2 (C2)	chr17:35,632,289-35,632,557	268	0
Control CRE_3 (C3)	chr17:35,633,285-35,633,418	133	0
ControlCRE_4 (C4)	chr17:35,633,801-35,633,934	133	0
sgRNAs targeting GFP (positive controls)	NA	NA	118
Non-targeting sgRNAs (negative controls)	NA	NA	1984

c

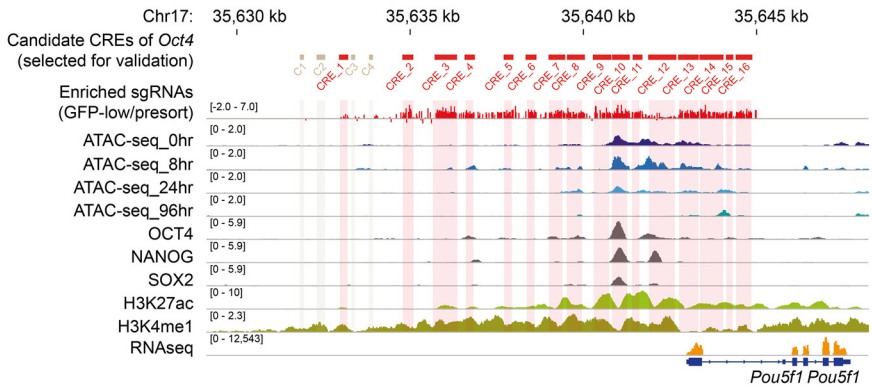

d

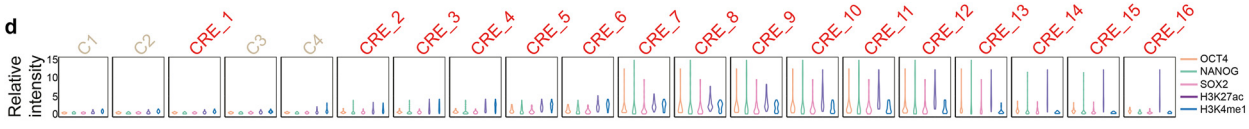

e

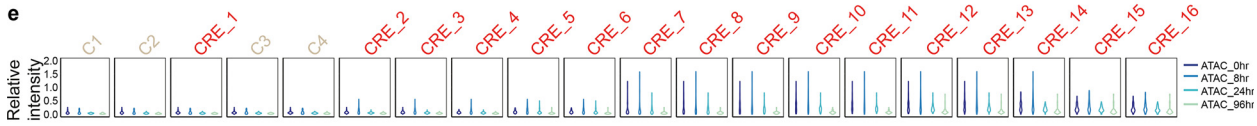

f

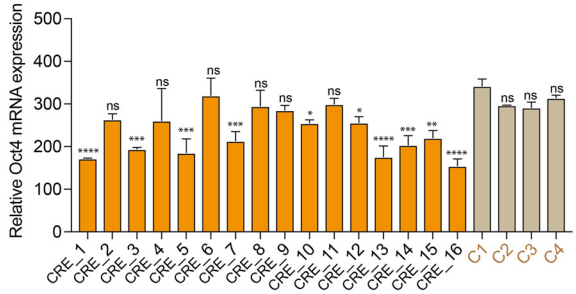

expression, compared with deletions of known distal and proximal enhancers (CREs 10 and 12) of *Oct4* (Fig. 2*f*). However, "regulatory features," such as co-occupancy of ESC-TFs (OCT4, NANOG, and SOX2–ONS), enhancer histone marks (H3K27ac and H3K4me1), and dynamic open chromatin regions (ATAC-Seq peaks at 0 h compared with 24, 96 h), were more prominent at CREs 7, 10, and 12 compared with CREs 1, 3, and 5 (Fig. 2 (*c–e*) and Fig. S3 (*b* and *c*)). Moreover, deletions of CREs 13–16 (present at the promoter region of *Oct4*) showed a significant reduction in Oct4 expression, as expected (Fig. 2*f*). Nonetheless, only CREs 13 and 14 showed substantial co-occupancy of ONS, H3K27ac, and dynamic open chromatin regions, as compared with other CREs present at the *Oct4* promoter (Fig. 2 (*c–e*) and Fig. S3 (*b* and *c*)). In contrast, deletions of control CREs (C1–C4) led to no significant changes in Oct4 expression (Fig. 2*f*). Additionally, control CREs exhibited low-level co-occupancy of ONS, H3K27ac, H3K4me1, and dynamic open chromatin regions (Fig. 2 (*d* and *e*) and Fig. S3 (*b* and *c*)). These data confirm the existence of multiple "active" CREs (active REs depict REs that reduce the Oct4 expression upon their deletions), including newly identified active CREs of the *Oct4*. Yet some active CREs fail to display recognized regulatory features (*i.e.* without of any co-occupancy of TFs, enhancer histone marks, and open chromatin regions), as described recently (26, 28), suggesting that a subset of functionally active REs may lack typical regulatory features.

Deletions of eight TREs (TREs 1, 2, 3, 4, 7, 9, 11, and 12) of 12 candidates showed a significant reduction in Oct4 expression to various extents (Fig. 3*e*). Nonetheless, all 12 TREs were co-occupied with ONS, H3K27ac, and H3K4me1 enhancer marks and exhibited dynamic open chromatin regions (Fig. 3 (*c* and *d*) and Fig. S4 (*b* and *c*)), as all of the candidate TREs (TREs 1–12) were short-listed for validation based on their regulatory features. Conversely, control TREs lack typical regulatory features (Fig. 3, *c* and *d*), and deletion did not affect Oct4 expression (Fig. 3*e*). Moreover, neighboring genes of most of the validated active TREs were lowly expressed in mESCs (Fig. S4*d*), indicating that these genes may not be critical for mESC state maintenance. Importantly, we observed that the reduction of Oct4 expression was greater for the majority of active CREs than active TREs upon their deletions (Figs. 2*f* and 3*e*). This suggests that CREs generally contribute more than TREs to control overall *Oct4* gene expression. Taken together, these data demonstrate the reliability and robustness of the ctSCAN-SMS screen to identify new candidate REs of the *Oct4* in a high-throughput manner. Moreover, we confirm that a subset of these newly identified candidate CREs and TREs are functionally active REs of the *Oct4* gene, and CREs are more active compared with TREs.

Cis- and trans-regulation of the Oct4 gene expression

REs (particularly enhancers) physically interact with gene promoters and control transcription (36). Chromosome conformation capture–based methods—4C, Hi-C, capture Hi-C, ChiA-PET, and HiChIP—have been utilized to identify physical contacts between promoters and REs (enhancers) (4). To interrogate the potential mechanisms by which candidate CREs and TREs regulate *Oct4* gene expression, we examined interactions between REs (CREs and TREs) and the *Oct4* promoter using published 4C-Seq data. These data were generated to study intrachromosomal and interchromosomal interactions between REs and the *Oct4* promoter at a genome-wide scale (37). We used Oct4-234 (a region at ~1.5 kb upstream of the TSS of Oct4) as a "viewpoint," as described previously (Fig. S5*a*) (37). Next, "contact frequencies" were calculated between the viewpoint and CREs (using a 1-kb resolution window, surrounding the 30-kb region of the *Oct4* gene locus) (Fig. 4, *a* and *c*), as well as between the viewpoint and TREs (using a 50-kb resolution window, surrounding each of the TREs) (Fig. 4*b*). This analysis revealed ranges of contact frequencies between functionally validated active CREs/TREs and the *Oct4* promoter (Figs. 2*f*, 3*e*, and 4 (*a* and *b*)). For example, functionally validated active CREs, including CREs 3, 5, and 7 (newly identified CREs), CREs 10 and 12 (previously known as distal and proximal enhancers of *Oct4*), and CREs 13–16 (residing at the promoter region of *Oct4*) demonstrated intrachromosomal interactions with the *Oct4* promoter (Fig. 4, *a* and *c*). Established enhancers, such as CREs 10 and 12, showed higher contact frequencies compared with newly identified CREs 3, 5, and 7 (Fig. 4, *a* and *c*). However, active CRE 1 and control CREs (C1–C4) did not show significant interactions with the *Oct4* promoter (Fig. 4, *a* and *c*). In contrast, among functionally validated active TREs 1, 2, 3, 4, 7, 9, 11, and 12, only a minority (TREs 2, 3, 4, and 11) displayed higher interchromosomal interactions (compared with control TRE) with the *Oct4* promoter (Fig. 4*b*).

Likewise, a high-resolution Micro-C (micrococcal nuclease–based Hi-C assay that captures genome-wide 3D chromatin organization/contact frequencies at single-nucleosome resolution (~100–200 bp)) from mESCs (38), displayed ranges of intrachromosomal interactions between active CREs and the *Oct4* promoter (Fig. S5, *b* and *c*). Further, these data evaluated all other intrachromosomal interactions between any two genomic loci around the ~20-kb region of the *Oct4* gene locus at 200 bp resolution (Fig. S5*b*). In addition, interchromosomal interactions were also observed between a few active TREs

Figure 2. Identification and dissection of active CREs of the *Oct4* gene. *a*, dot plot analysis demonstrates the enrichment score of each sgRNA by comparing its frequency in the GFP-low cells with that in the pre-sort cells. 16 candidate CREs were identified based on the mean enrichment score (mean $\log_2$FC) of sgRNAs per CRE. Four control CREs do not contain any sgRNAs. sgRNAs targeting GFP (*green*) and nontargeting sgRNAs (*black*) were used as positive and negative controls, respectively. *b*, a list of identified candidate CREs of the *Oct4* gene. *c*, genomic tracks exhibit open chromatin regions/ENs by ATAC-Seq at different time points (0, 8, 24, and 96 h) from undifferentiated to differentiated mESC state; co-occupancy of ESC-TFs (OCT4, NANOG, and SOX2) and enhancer histone marks (H3K27ac and H3K4me1) is also displayed at the mouse *Oct4* locus. RNA-Seq shows the *Oct4* expression. *d*, violin plots outlining the binding dynamics of OCT4, NANOG, SOX2, H3K27ac, and H3K4me1 within the different CREs of *Oct4*. *e*, dynamic changes of open chromatin regions/ENs measured by ATAC-Seq (using the 0-, 8-, 24-, and 96-h time points from undifferentiated to differentiated mESC state) within the CREs of *Oct4*. *f*, endogenous Oct4 mRNA expression levels quantified upon deletion of individual CREs of *Oct4*. Oct4 mRNA levels were normalized to GAPDH. Data are represented as mean ± S.E. (*error bars*) ($n = 3$); *p* values were calculated using analysis of variance. *, $p < 0.05$; **, $p < 0.01$; ***, $p < 0.001$; ****, $p < 0.0001$; *ns*, nonsignificant.

a

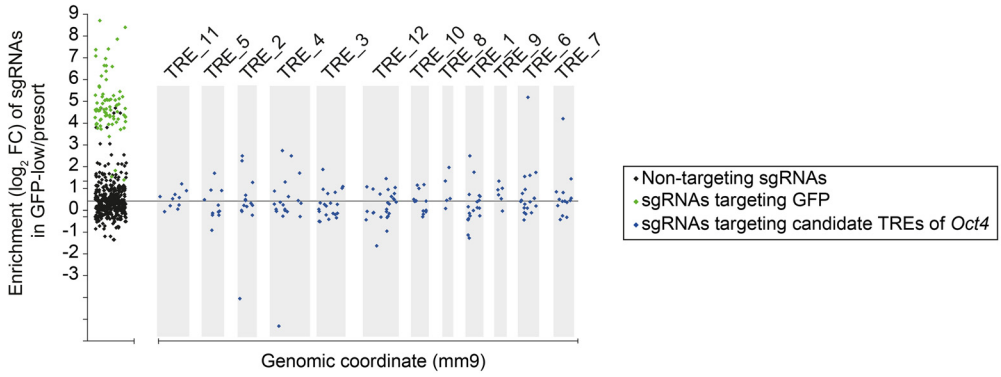

b

List of candidate TREs of the *Oct4* gene

Based on HMM based enrichment scores of sgRNAs.
All the sgRNAs must have off-target score >10.
TREs must possess at least 4 sgRNAs with mean enrichment scores (mean log2FC) >0.5, P-values <0.0001.
TREs should co-occupy with ESC-TFs (OCT4, NANOG, SOX2), enhancer histone marks (H3K27ac, H3K4me1) and dynamic open chromatin regions.

Candidate TREs	Genomic locations	Length (bp)	No. of sgRNAs
TRE_1	chr14:59,989,540-59,989,621	81	20
TRE_2	chr4:71,807,347-71,807,416	69	12
TRE_3	chr9:74,696,403-74,696,575	172	21
TRE_4	chr9:13,978,361-13,978,560	199	20
TRE_5	chr4:13,023,503-13,023,629	126	11
TRE_6	chr19:53,534,741-53,534,849	108	19
TRE_7	chrX:130,208,023-130,208,140	117	14
TRE_8	chr12:42,828,460-42,828,512	52	5
TRE_9	chr18:82,062,626-82,062,657	31	6
TRE_10	chr11:63,347,393-63,347,468	75	11
TRE_11	chr1:7,722,856-7,723,033	177	10
TRE_12	chr10:7,365,884-7,366,087	203	25
TRE_control	chr1:120,957,901-120,958,247	346	0
sgRNAs_GFP (positive controls)	NA	NA	118
sgRNAs_non-targeting (negative controls)	NA	NA	1984

c

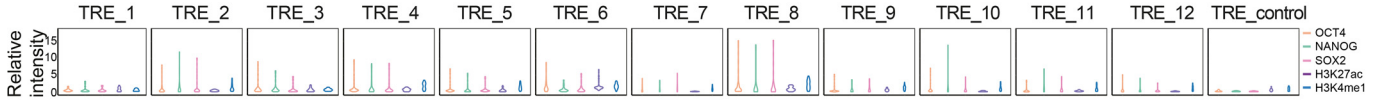

d

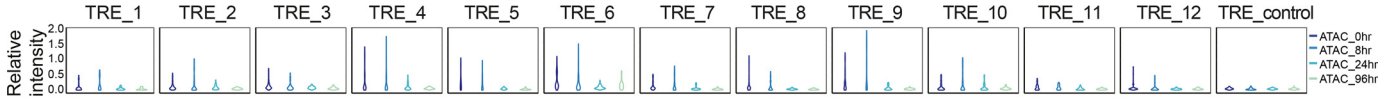

e

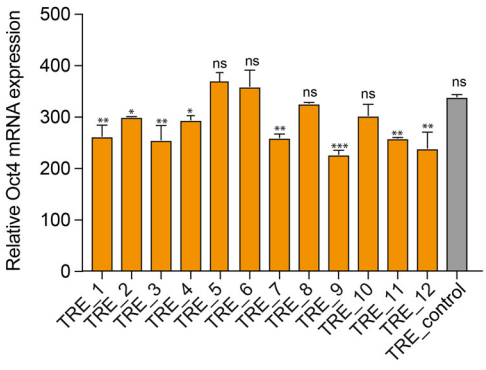

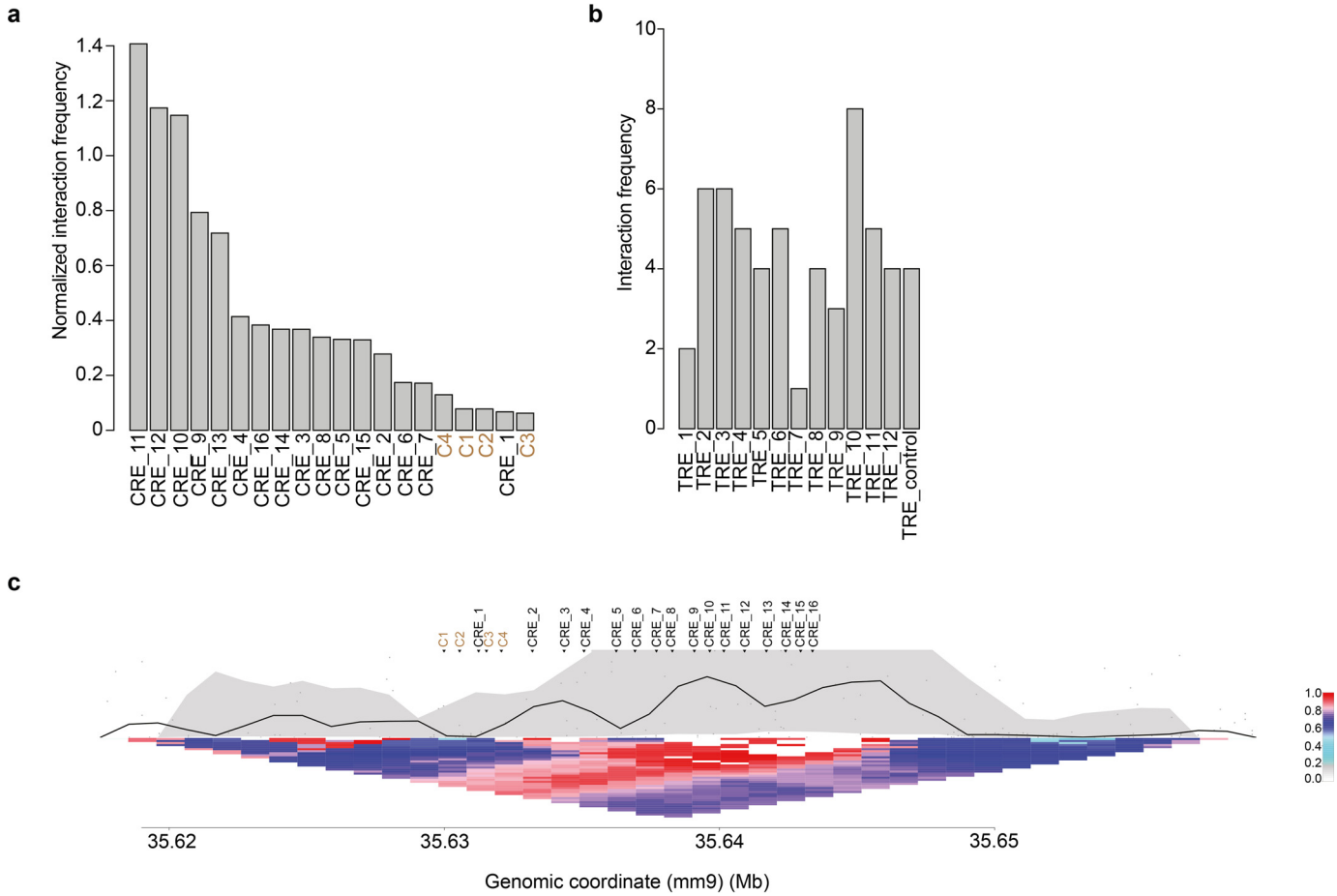

Figure 4. Physical interactions between CREs, TREs, and the *Oct4* promoter in *Oct4* gene regulation. *a*, 4C-Seq data represent normalized interaction frequencies between CREs and the *Oct4* promoter. The interaction/contact frequencies between CREs and the *Oct4* promoter were measured at a 1-kb resolution window. *b*, interaction/contact frequencies between TREs and the *Oct4* promoter quantified at a 50-kb resolution window. *c*, contact profile of CREs and the *Oct4* promoter at a 1-kb resolution window. *Bottom triangle*, heat map of normalized contact frequencies between 1-kb bins represented with the *color codes* (the highest is 1 with *red*; the lowest is 0 with *white*). In the *top part*, the *black line* (within the *gray region*) represents the normalized median contact frequencies between a locus and the viewpoint. The *gray region* exhibits the 20th to 80th percentile of the normalized contact frequencies.

(TREs 4 and 11) and the *Oct4* promoter (Fig. S5*d*). Both 4C-Seq and Micro-C data showed greater contact frequencies of active CREs compared with active TREs with the *Oct4* promoter, and a greater number of active CREs compared with active TREs physically interacted with the *Oct4* promoter (Fig. 4 (*a–c*) and Fig. S5 (*b–d*)). Taken together, our data suggest that a subset of active CREs and TREs physically interact with the *Oct4* promoter at different frequencies as they influence the *Oct4* transcriptional output.

Conserved functionally active CREs and TREs of the Oct4 gene

Recent studies demonstrate that the majority of species-specific REs/ENs evolved *de novo* from ancestral DNA regulatory sequences (16, 39). Also, evidence implies that loss or gain of REs (called RE turnover) takes place during evolution (17). To understand the importance of validated active CREs and TREs of the mouse *Oct4* gene in evolutionary turnover, we analyzed their regulatory sequence conservation. Active CREs 3 and 5, CREs 10 and 12 (known distal and proximal ENs), and CREs 13–16 (present within the promoter) demonstrated significant conservation between mice and primates, including humans (Fig. 5*a*), whereas active CREs 1 and 7 did not show appreciable sequence conservation between mice and primates (Fig. 5*a*). Compared with active CREs, only a small subset of active TREs (TREs 3 and 4) showed significant sequence conservation between mice and primates (Fig. 5, *b* and *c*). These observations suggest that active CREs are more critical than active TREs for *Oct4* expression in mice and primates (including humans) during evolution.

Figure 3. Identification and validation of active TREs of the *Oct4* gene. *a*, dot plot analysis displays the enrichment score of each sgRNAs by comparing its frequency in the GFP-low cells with that in the pre-sort cells at the selected candidate 12 TREs. *b*, list of identified candidate TREs of the *Oct4* gene. *c*, binding dynamics of OCT4, NANOG, SOX2, H3K27ac, and H3K4me1 represented within the TREs of *Oct4*. *d*, ATAC-Seq demonstrates the changes in open chromatin regions/ENs from undifferentiated to differentiated mESC state (0, 8, 24, and 96 h) within the TREs. *e*, quantitative RT-PCR data illustrate the mRNA expression changes of endogenous *Oct4* upon deletion of individual TREs of *Oct4*. Oct4 mRNA levels were normalized to GAPDH. Data are represented as mean ± S.E. (*error bars*) ($n = 3$); *p* values were calculated using analysis of variance. *, $p < 0.05$; **, $p < 0.01$; ***, $p < 0.001$; *ns*, nonsignificant.

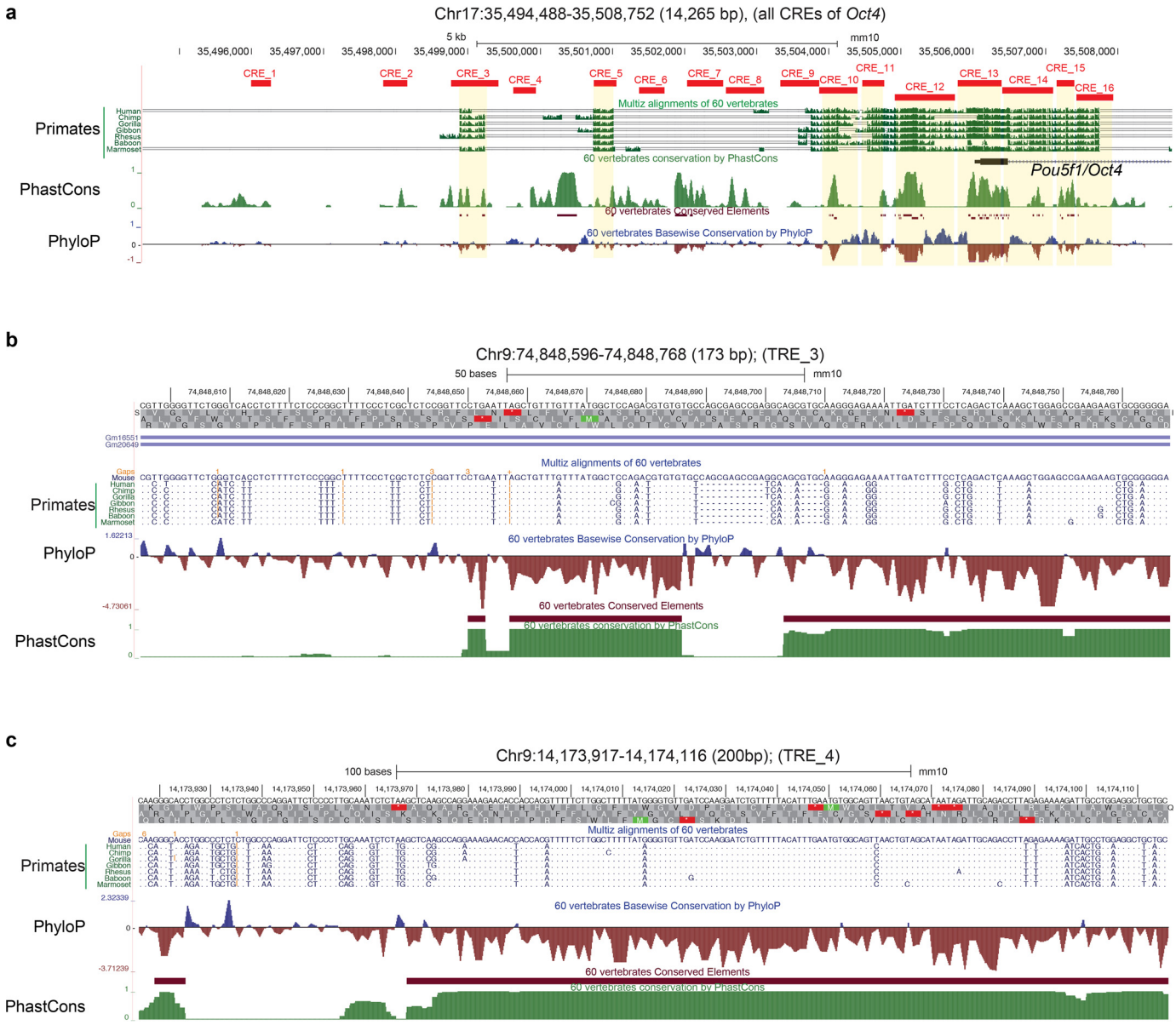

Figure 5. Conserved active CREs and TREs of the *Oct4* gene. *a*, orthologous sequences from the representative primates (including humans) are listed around the ~12-kb region of the mouse *Oct4* locus. CREs of the mouse *Oct4* are labeled with *solid red bars*. PhyloP and PhastCons estimate evolutionary conservation among 60 vertebrates. *b* and *c*, orthologous sequences from the representative primates (including humans) are listed at the active TRE-3 (*b*) and TRE-4 (*c*) regions of the mouse *Oct4*. PhyloP and PhastCons estimate evolutionary conservation among 60 vertebrates.

Next, we analyzed regulatory sequence conservation of previously identified high-confidence CREs (−449, −571, and −694) of human *OCT4*. These CREs are located distally between ~450 and 700 kb upstream of the human *OCT4* TSS and physically interact with the *OCT4* gene (28). We found that these human CREs are also evolutionarily conserved at the upstream regions of the mouse *Oct4* locus (Fig. S6).

Taken together, our comprehensive comparative genomic analysis shows that a larger subset of active CREs compared with active TREs of *Oct4* are well-conserved between mice and primates, including humans. These observations support the existence of both conserved and nonconserved REs of *Oct4* among mice and primates (including humans), which is consistent with "RE turnover/divergence" (gain and loss of REs) at the *Oct4* locus during evolution that may be critical for positive selection, as proposed earlier (17, 39).

Discussion

A handful of modest scale CRISPR-Cas9–mediated functional screens (using hundreds to thousands of sgRNAs) have been performed to target specific noncoding CREs of a gene(s) of interest (24–26, 29, 40). These screens successfully identified functional CREs of the target gene(s). In the context of identification of CREs of the *OCT4* gene, a previous CRISPR-Cas9–mediated screen was performed to target 174 candidate CREs of *OCT4* within its 1-MB topological associated domain in human ESCs; it revealed four temporary CREs and two known proximal CREs. The temporary CREs showed "transient"

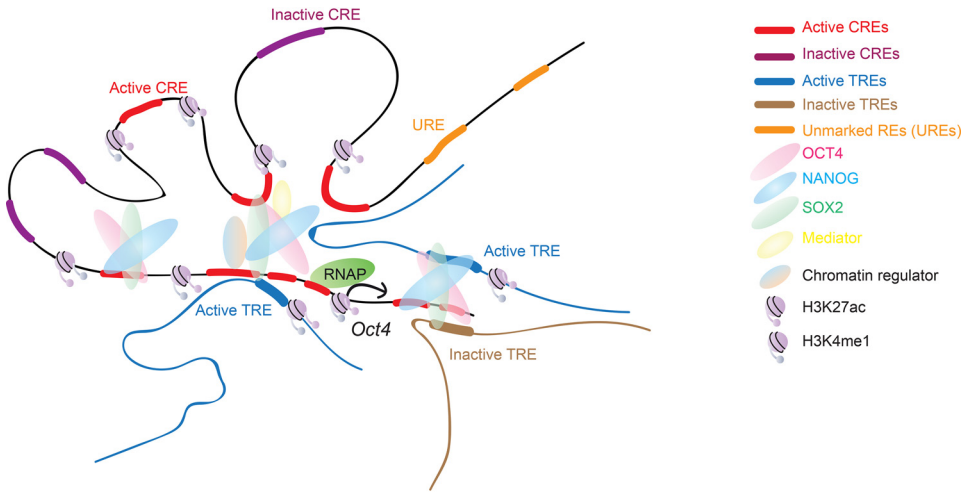

Figure 6. Model representing the detailed functions of CREs and TREs in *Oct4* gene regulation. The proposed model describes the existence of multiple active CREs (*red*) and TREs (*blue*) of the *Oct4* locus in mESCs. However, not all of the active REs have regulatory features (*i.e.* co-occupancy of ESC-TFs (OCT4, NANOG, and SOX2), active enhancer histone marks (H3K27ac and H3K4me1), and open chromatin regions), which are termed unmarked REs (*UREs*). Also, a subset of active REs physically interacts with the *Oct4* promoter through intrachromosomal (for CREs) and interchromosomal (for TREs) interactions. Taken together, it suggests that active REs act beyond their regulatory features and physically contact the *Oct4* promoter to control the transcriptional output of the *Oct4* gene.

enhancer regulatory activity in *OCT4* gene expression (27). However, the functional relevance of these temporary CREs is uncertain in human *OCT4* gene regulation. Furthermore, another CRISPR-Cas9–mediated screen was performed by the same group using a different strategy, called CREST-Seq. This method employed 11,570 paired sgRNAs to introduce deletions to target 2 Mb surrounding the *OCT4* locus in human ESCs, which created 2-kb deletions on average with an overlap of 1.9 kb between two adjacent deletions. This screen identified a total of 45 CREs, of which 17 CREs (with regulatory features) reside at the promoters of "unrelated" genes (intrachromosomally) that act as typical enhancers of the *OCT4* gene (28). Our study employed ctSCAN-SMS—an unbiased, high-resolution, high-throughput screening approach using 1,827 sgRNAs to target CREs and 70,480 sgRNAs to target TREs of the mouse *Oct4* gene (Fig. 1).

Previous CRISPR-Cas9 screens were focused on CREs of the target gene(s). In contrast, our screen was designed to identify both CREs and TREs. Indeed, we discovered 16 CREs (including 10 novel CREs) and 12 novel TREs of the murine *Oct4* gene, as potential candidate REs (Figs. 2*a* and 3*a*). Furthermore, deletion studies confirmed that the majority of these CREs (10 of 16) and TREs (8 of 12) are functionally active in controlling the *Oct4* expression. Overall, CREs are more functionally active than TREs (Figs. 2*f* and 3*e*). In addition, we showed that a subset of these active CREs and TREs physically interacts with the *Oct4* promoter to different extents through intra- and interchromosomal interactions, respectively (Fig. 4 and Fig. S5). Notably, a greater number of active CREs, compared with active TREs, physically interact with the *Oct4* promoter. Moreover, the interactions between active CREs (compared with active TREs) and the *Oct4* promoter are more prominent (Fig. 4 and Fig. S5). Nonetheless, "enhancer activities" of several active CREs/TREs are not directly correlated to their physical contact frequencies with the *Oct4* promoter (Figs. 2*f*, 3*e*, and 4 and Fig. S5). Interestingly, we found that several active CREs (CREs 1, 3, and 5) lack typical regulatory features (Figs. 2 (*d–f*) and 6); this supports earlier studies that found that unmarked REs (*UREs*) without typical regulatory features may play critical roles in transcriptional output (26, 28). Moreover, comparative genomics analysis revealed that numerous active CREs and active TREs (a greater number of active CREs than active TREs) of *Oct4* are evolutionarily conserved between mice and primates (including humans) (Fig. 5). However, we also observed divergence of *Oct4* REs among mice and primates (including humans), which may account for the vital roles of "RE turnover" during evolution (3, 39).

Several studies demonstrate that "multiple REs" act either in a cooperative or competitive fashion to control transcriptional output (39). Our study identified multiple active REs of *Oct4* and revealed a spectrum of regulatory activities of "individual" CREs and TREs in *Oct4* gene expression (Figs. 2*f* and 3*e*). Further systematic studies will be required to elucidate how multiple REs function combinatorially to control *Oct4* transcriptional output. In conclusion, we have demonstrated the utility of ctSCAN-SMS as an approach to identify functional REs of a gene locus and dissect their regulatory contributions to the transcriptional output of a target gene within its normal chromosomal context.

Experimental procedures

mESCs

mESCs were cultured in mouse ESC medium that contains Dulbecco's modified Eagle's medium (Thermo Fisher Scientific) supplemented with 15% fetal calf serum (Merck Millipore), 0.1 mM β-mercaptoethanol (Sigma–Aldrich), 2 mM L-glutamine (Thermo Fisher Scientific), 0.1 mM nonessential amino acid (Thermo Fisher Scientific), 1% of nucleoside mix (Merck Millipore), 1000 units/ml recombinant leukemia inhibitory factor (LIF/ESGRO) (Merck Millipore), and 50 units/ml penicillin/

streptomycin (Thermo Fisher Scientific), as described previously (32, 41). mESCs were cultured at 37 °C, 5% CO_2.

Mouse RE CRISPR-Cas9 pooled library design for the ctSCAN-SMS

For this study, we selected a list of putative 8,563 EN and 231 SE REs from the mESCs, as described previously (30). First, we generated ATAC-Seq (10) data from WT mESCs and mapped within all of the putative EN and SE REs to identify open chromatin regions as well as high-confidence REs. Next, ±100 bp (200 bp) around the center of the ATAC-Seq peaks were obtained from the high-confidence REs. In total, we identified 2,613 REs for targeting. All possible sgRNAs (20 nt) were designed upstream of the *S. pyogenes* Cas9 NGG-PAM sequences at these defined REs (2,613), which created 70,480 sgRNAs with a median gap of 5 bp between adjacent genomic cleavages. Because these EN and SE REs were distributed in *trans* of the *Oct4* gene locus, we called these REs *trans*-REs (TREs). Likewise, 1,827 sgRNAs were designed prior to all possible NGG-PAM sequences at the adjacent ~12-kb (−10 to +2 kb of the TSS of *Oct4*) region of the mouse *Oct4* gene locus to systematically dissect the REs of *Oct4*. As these REs reside adjacent to the *Oct4* gene locus, they are called *cis*-REs (CREs). We also included 2,000 NT sgRNAs as negative controls and 119 sgRNAs targeting GFP of the *Oct4*-GFP reporter and 150 sgRNAs targeting coding sequence of mESC-TFs as positive controls. Altogether, the RE CRISPR-Cas9 pooled library contained a total of 74,576 sgRNAs.

RE CRISPR-Cas9 pooled library construction for the ctSCAN-SMS

All of the sgRNA oligonucleotides of the library were synthesized as described previously (32) using a B3 synthesizer (CustomArray, Inc.), pooled together, PCR-amplified and cloned into Esp3I-digested plentiGuide-Puro (Addgene plasmid ID: 52963) lentiviral vector, using a Gibson assembly master mix (New England Biolabs). Gibson assembly products were transformed into electrocompetent cells (E. cloni, Lucigen) and plated on 245 × 245-mm square LB-agar plates to obtain the sufficient number of bacterial colonies at a ~50× library coverage. Bacterial colonies were collected from the plates, genomic DNA was isolated, and plasmid libraries were prepared for high-throughput sequencing to confirm the representation of individual sgRNAs in the RE CRISPR-Cas9 pooled library.

Lentiviral library production

HEK293T cells were seeded onto 15-cm dishes ~24 h prior to transfection. Cells were transfected at 80% confluence in 16 ml of medium with 8.75 μg of VSVG, 16.25 μg of psPAX2, and 25 μg of the RE CRISPR-Cas9 pooled lentiviral plasmids, using 150 μg of linear polyethylenimine (Sigma–Aldrich). Medium was changed with fresh medium, 16–24 h after transfection. Lentiviral supernatant was collected at 48 and 72 h post-transfection and subsequently concentrated by ultracentrifugation (24,000 rpm, 4 °C, 2 h) (Beckman Coulter SW32).

CRISPR-Cas9–mediated ctSCAN-SMS in mESCs

Oct4-GFP reporter mESCs with stably expressed Cas9 were transduced with an RE CRISPR-Cas9 pooled lentiviral library at low MOI to avoid more than one lentiviral integration per cell. Test transductions were performed to estimate the viral titration and transduction rate. Briefly, 300,000 *Oct4*-GFP + Cas9 mESCs were plated per well of a 12-well plate. After 24 h, different amounts (1, 2, 4, 6, and 8 μl) of the lentiviral library were added to the cells. 10 μg/ml blasticidin (InvivoGen) and 1 μg/ml puromycin (Sigma–Aldrich) were added 24 h after the transduction to select for lentiviral library integrants (puromycin-resistant) in cells with Cas9 (blasticidin-resistant). Cells were selected for the next 3–4 days. The same number of cells were seeded as a control but not infected with lentiviral library and not treated with blasticidin and puromycin. The number of blasticidin- and puromycin-resistant cells and control cells were counted to calculate the viral titer and transduction rate (to achieve 30%).

For the actual screen, we seeded ~112 million (~75,000 sgRNAs in the pooled library, with 500× coverage, for a 30% transduction rate) *Oct4*-GFP + Cas9 mESCs in the same format (*i.e.* 300,000 cells/well of the 12-well plate) for each independent screening replicate. The lentiviral library was added to each well of a 12-well plate to achieve a 30% transduction rate with low MOI (MOI 0.1) to make sure each infected cell obtained one viral particle. 24 h post-transduction, fresh mESC medium was added to the cells with 10 μg/ml blasticidin (InvivoGen) and 1 μg/ml puromycin (Sigma–Aldrich) and selected for 4 days. These selected cells were used to sort the "GFP-low" cells. The "pre-sort" cells were collected before sorting and used as a control. Genomic DNA was isolated from both the "GFP-low" and "pre-sort" cell populations, and libraries were prepared for deep sequencing to enumerate the presence of sgRNAs in these cell populations as described previously (32). The screening was performed in biological triplicates.

Deletion of CREs and TREs of Oct4 in mESCs

Paired sgRNAs (5′ and 3′ sgRNAs) were designed to target both the ends of each selected candidate RE to create a deletion. Both the sgRNAs were cloned into lentiGuide-plasmid that carries Cas9 and mCherry, using the Golden Gate cloning approach as described previously (32). 1,000,000 WT (J1) mESCs were transfected with 1 μg of each 5′ and 3′ sgRNA-Cas9-mCherry plasmids using Lipofectamine 2000 (Thermo Fisher Scientific). After 24 h of transfection, mCherry-positive cells were sorted; at least 50,000–100,000 mCherry-positive cells were collected either to isolate the total RNA for measuring the endogenous Oct4 mRNA expression levels by quantitative RT-PCR or to perform the genotyping PCR for checking deletions of targeted REs.

Flow cytometry

Cells were dissociated using trypsin and washed with 1× PBS, followed by sorting. (i) During the CRISPR-Cas9 screening, *Oct4*-GFP reporter mESCs were sorted based on GFP-low intensity after the transduction with the RE CRISPR-Cas9 pooled library; (ii) to quantify the *Oct4* mRNA expressions

upon deletions of CREs and TREs, their targeting sgRNAs-mCherry–positive cells were sorted.

RNA isolation and RT-qPCR

DNA-free total RNA was isolated from mESCs using the RNeasy Mini Kit (Qiagen), and cDNA was prepared using the iScript cDNA synthesis kit (Bio-Rad). RT-qPCR was performed using iQ SYBR Green Supermix (Bio-Rad) on the Bio-Rad iCycler RT-PCR detection system.

ctSCAN-SMS screen data analysis

sgRNA sequences present in the GFP-low and pre-sort pools were enumerated. Enrichment was determined by the $\log_2$ transformation of the median number of occurrences of a particular sgRNA in the GFP-low pool divided by the median number of occurrences of the same sgRNA in the pre-sort pool across the best two biological screen replicates.

ATAC-Seq experiment and data analysis

ATAC-Seq was performed according to the previously described protocol (10), with some modifications. Briefly, each library was started with 50,000 cells, which were washed with 1× PBS and permeabilized with 50 μl of lysis buffer (10 mM Tris, pH 7.4, 10 mM NaCl, 3 mM $MgCl_2$, 0.1% IGEPAL) at 40 °C by resuspension. Cells were centrifuged at 500 × *g* for 10 min at 40 °C to pellet the nuclei. The resulting nuclei were resuspended in 50 μl of transposition reaction buffer (25 μl of 2× TD buffer from the Nextera kit (Illumina), 2.5 μl of Tn5 transposase enzyme from the Nextera kit (Illumina), and 22.5 μl of nuclease-free water) and incubated at 37 °C for 90 min for chromatin tagmentation. Next, DNA was purified using the Qiagen MinElute PCR purification kit and eluted in 10 μl of nuclease-free water. PCR amplification was performed using Nextera primers (Illumina) to make the libraries for deep sequencing.

The obtained deep sequencing data in .FASTQ format were inspected first by FASTQC. Next, reads were trimmed for adapters using Trimmomatic (42). The resulting fastq files were aligned with Bowtie2 (43) with the following options: local × 2000. Peaks were called with MACS2 (44) with the following options: callpeak –gsize mm –nomodel –shift -100 –extsize 200 –call-summit.

4c-Seq data analysis

The normalized interaction frequencies between CREs and *Oct4* promoter were measured based on the 4C-Seq pipeline (37) with some modifications. Normalized interaction frequencies between CREs and *Oct4* promoter (Oct-234 used as a viewpoint) was quantified at a higher resolution (1-kb resolution window compared with previous analysis, which used a 7-kb resolution window). We used the following command: perl 4cseqpipe.pl -dopipe -ids 1 -fastq_fn Oct4/fastq/Oct4_234.fastq -convert_qual 1 -calc_from 35620000 -calc_to 35660000 -stat_type median -trend_resolution 1000 -figure_fn Oct4_234_1K.pdf -feat_tab rawdata/Oct4_234_features.txt. The contact frequencies between TREs and *Oct4* promoter were calculated based on the number of contacts between the *Oct4* promoter (Oct4-234 used as a view point) and a 50-kb region centered at each TRE, using the bedtools intersect command.

Micro-C data analysis

Raw Micro-C data from mESCs was downloaded from GEO (GSE130275) (38). Samples were processed with a standard juicer pipeline (45), using the mm9 mouse genome. Reads from all 37 samples were merged together (after removal of duplicates). This resulted in more than 4 billion contacts, allowing the creation of a Hi-C file at a very high (200-bp) resolution. For CRE contacts, the chr17 intrachromosomal contact map was processed using an in-house tool to produce normalized observed/expected counts. These counts were used for the creation of a heat map/matrix and bar plot. For each CRE (including *Oct4* TSS), all 200-bp bins overlapping the loci were used. For TRE contacts, a whole-genome 1-kb resolution contact map was created and balanced using our in-house C++ code (this is the GW_SCALE normalization available in juicer_tools_1.22.01.jar).[12] These counts were used for the creation of the bar plot. In this case, the *Oct4* promotor was defined as ±3 kb of TSS, and TREs were used 200 kb bin centered at the particular TRE. The heat map was generated using a heatmap.2 R function from the gplots package, and bar plots were generated using a bar plot R function.

Data availability

All of the high-throughput sequencing data from this study have been submitted to the NCBI Gene Expression Omnibus (GEO) under accession number GSE140911. ChIP-Seq and RNA-Seq data used are from GSE113335 (32) and GSE43231 (41).

Acknowledgments—We thank the Monash University FACS core facility. We thank Xiaofeng Wang for Illumina HiSeq2500 high-throughput sequencing at Harvard Medical School as well as the Genewiz high-throughput sequencing facility, China.

Author contributions—M. C. C., P. T., Y. K., L. P., and P. P. D. data curation; M. C. C., Y. K., and L. P. software; M. C. C., M. O., Y. K., L. P., and P. P. D. formal analysis; M. C. C., P. T., M. J. B., L. H. W., S. H. O., and P. P. D. investigation; M. C. C., M. O., Y. K., and L. P. visualization; M. C. C., S. H. O., and P. P. D. writing-original draft; M. C. C., P. T., S. H. O., and P. P. D. writing-review and editing; P. T. and M. J. B. validation; P. T., M. J. B., L. P., and P. P. D. methodology; S. J. T., S. L., and L. P. resources; S. J. T., S. H. O., and P. P. D. project administration; S. H. O. and P. P. D. conceptualization; S. H. O. and P. P. D. supervision; S. H. O. and P. P. D. funding acquisition.

Funding and additional information—This work was supported by National Health and Medical Research Council (NHMRC) of Australia Grants APP1159461 and APP1182804 (to P. P. D.) and National Human Genome Research Institute (NHGRI) Career

[12] M. C. Canver, P. Tripathi, M. J. Bullen, M. Olshansky, Y. Kumar, L. H. Wong, S. J. Turner, S. Lessard, L. Pinello, S. H. Orkin, and P. P. Das, manuscript in preparation.

Development Award R00HG008399 and Genomic Innovator Award R35HG010717 (to L. P.). S. H. O. is an Investigator of the Howard Hughes Medical Institute (HHMI). The content is solely the responsibility of the authors and does not necessarily represent the official views of the National Institutes of Health.

Conflict of interest—The authors declare that they have no conflicts of interest with the contents of this article.

Abbreviations—The abbreviations used are: RE, regulatory element; CRE, *cis*-RE; TRE, *trans*-RE; TF, transcription factor; ctSCAN-SMS, *cis*- and *trans*-regulatory elements scanning through saturating mutagenesis and sequencing; ESC, embryonic stem cell; mESC, mouse ESC; EN, enhancer; SE, superenhancer; sgRNA, single guide RNA; TSS, Transcription start site; MOI, multiplicity of infection; FC, -fold change; H3K27ac, histone H3 Lys-27 acetylation; H3K4me1, histone H3 Lys-4 monomethylation; HMM, hidden Markov model; GAPDH, glyceraldehyde-3-phosphate dehydrogenase.

References

1. ENCODE Project Consortium, (2012) An integrated encyclopedia of DNA elements in the human genome. *Nature* **489,** 57–74
2. Cech, T. R., and Steitz, J. A. (2014) The noncoding RNA revolution-trashing old rules to forge new ones. *Cell* **157,** 77–94 CrossRef Medline
3. Miele, A., and Dekker, J. (2008) Long-range chromosomal interactions and gene regulation. *Mol. Biosyst.* **4,** 1046–1057 CrossRef Medline
4. Elkon, R., and Agami, R. (2017) Characterization of noncoding regulatory DNA in the human genome. *Nat. Biotechnol.* **35,** 732–746 CrossRef Medline
5. Visel, A., Blow, M. J., Li, Z., Zhang, T., Akiyama, J. A., Holt, A., Plajzer-Frick, I., Shoukry, M., Wright, C., Chen, F., Afzal, V., Ren, B., Rubin, E. M., and Pennacchio, L. A. (2009) ChIP-seq accurately predicts tissue-specific activity of enhancers. *Nature* **457,** 854–858 CrossRef Medline
6. Mouse ENCODE Consortium, Stamatoyannopoulos, J. A., Snyder, M., Hardison, R., Ren, B., Gingeras, T., Gilbert, D. M., Groudine, M., Bender, M., Kaul, R., Canfield, T., Giste, E., Johnson, A., Zhang, M., Balasundaram, G., *et al.* (2012) An encyclopedia of mouse DNA elements (Mouse ENCODE). *Genome Biol.* **13,** 418 CrossRef Medline
7. Roadmap Epigenomics Consortium, Kundaje, A., Meuleman, W., Ernst, J., Bilenky, M., Yen, A., Heravi-Moussavi, A., Kheradpour, P., Zhang, Z., Wang, J., Ziller, M. J., Amin, V., Whitaker, J. W., Schultz, M. D., Ward, L. D., *et al.* (2015) Integrative analysis of 111 reference human epigenomes. *Nature* **518,** 317–330 CrossRef Medline
8. Ernst, J., Kheradpour, P., Mikkelsen, T. S., Shoresh, N., Ward, L. D., Epstein, C. B., Zhang, X., Wang, L., Issner, R., Coyne, M., Ku, M., Durham, T., Kellis, M., and Bernstein, B. E. (2011) Mapping and analysis of chromatin state dynamics in nine human cell types. *Nature* **473,** 43–49 CrossRef Medline
9. Thurman, R. E., Rynes, E., Humbert, R., Vierstra, J., Maurano, M. T., Haugen, E., Sheffield, N. C., Stergachis, A. B., Wang, H., Vernot, B., Garg, K., John, S., Sandstrom, R., Bates, D., Boatman, L., *et al.* (2012) The accessible chromatin landscape of the human genome. *Nature* **489,** 75–82 CrossRef Medline
10. Buenrostro, J. D., Giresi, P. G., Zaba, L. C., Chang, H. Y., and Greenleaf, W. J. (2013) Transposition of native chromatin for fast and sensitive epigenomic profiling of open chromatin, DNA-binding proteins and nucleosome position. *Nat. Methods* **10,** 1213–1218 CrossRef Medline
11. Maurano, M. T., Humbert, R., Rynes, E., Thurman, R. E., Haugen, E., Wang, H., Reynolds, A. P., Sandstrom, R., Qu, H., Brody, J., Shafer, A., Neri, F., Lee, K., Kutyavin, T., Stehling-Sun, S., *et al.* (2012) Systematic localization of common disease-associated variation in regulatory DNA. *Science* **337,** 1190–1195 CrossRef Medline
12. Andersson, R., Gebhard, C., Miguel-Escalada, I., Hoof, I., Bornholdt, J., Boyd, M., Chen, Y., Zhao, X., Schmidl, C., Suzuki, T., Ntini, E., Arner, E., Valen, E., Li, K., Schwarzfischer, L., *et al.* (2014) An atlas of active enhancers across human cell types and tissues. *Nature* **507,** 455–461 CrossRef Medline
13. Farh, K. K.-H., Marson, A., Zhu, J., Kleinewietfeld, M., Housley, W. J., Beik, S., Shoresh, N., Whitton, H., Ryan, R. J. H., Shishkin, A. A., Hatan, M., Carrasco-Alfonso, M. J., Mayer, D., Luckey, C. J., Patsopoulos, N. A., *et al.* (2015) Genetic and epigenetic fine mapping of causal autoimmune disease variants. *Nature* **518,** 337–343 CrossRef Medline
14. Vierstra, J., Rynes, E., Sandstrom, R., Zhang, M., Canfield, T., Hansen, R. S., Stehling-Sun, S., Sabo, P. J., Byron, R., Humbert, R., Thurman, R. E., Johnson, A. K., Vong, S., Lee, K., Bates, D., *et al.* (2014) Mouse regulatory DNA landscapes reveal global principles of cis-regulatory evolution. *Science* **346,** 1007–1012 CrossRef Medline
15. Stergachis, A. B., Neph, S., Sandstrom, R., Haugen, E., Reynolds, A. P., Zhang, M., Byron, R., Canfield, T., Stelhing-Sun, S., Lee, K., Thurman, R. E., Vong, S., Bates, D., Neri, F., Diegel, M., *et al.* (2014) Conservation of trans-acting circuitry during mammalian regulatory evolution. *Nature* **515,** 365–370 CrossRef Medline
16. Villar, D., Berthelot, C., Aldridge, S., Rayner, T. F., Lukk, M., Pignatelli, M., Park, T. J., Deaville, R., Erichsen, J. T., Jasinska, A. J., Turner, J. M. A., Bertelsen, M. F., Murchison, E. P., Flicek, P., and Odom, D. T. (2015) Enhancer evolution across 20 mammalian species. *Cell* **160,** 554–566 CrossRef Medline
17. Siepel, A., and Arbiza, L. (2014) Cis-regulatory elements and human evolution. *Curr. Opin. Genet. Dev.* **29,** 81–89 CrossRef Medline
18. Melnikov, A., Murugan, A., Zhang, X., Tesileanu, T., Wang, L., Rogov, P., Feizi, S., Gnirke, A., Callan, C. G., Kinney, J. B., Kellis, M., Lander, E. S., and Mikkelsen, T. S. (2012) Systematic dissection and optimization of inducible enhancers in human cells using a massively parallel reporter assay. *Nat. Biotechnol.* **30,** 271–277 CrossRef Medline
19. Patwardhan, R. P., Hiatt, J. B., Witten, D. M., Kim, M. J., Smith, R. P., May, D., Lee, C., Andrie, J. M., Lee, S.-I., Cooper, G. M., Ahituv, N., Pennacchio, L. A., and Shendure, J. (2012) Massively parallel functional dissection of mammalian enhancers *in vivo*. *Nat. Biotechnol.* **30,** 265–270 CrossRef Medline
20. Mali, P., Yang, L., Esvelt, K. M., Aach, J., Guell, M., DiCarlo, J. E., Norville, J. E., and Church, G. M. (2013) RNA-guided human genome engineering via Cas9. *Science* **339,** 823–826 CrossRef Medline
21. Mojica, F. J. M., Díez-Villaseñor, C., García-Martínez, J., and Almendros, C. (2009) Short motif sequences determine the targets of the prokaryotic CRISPR defence system. *Microbiology (Reading)* **155,** 733–740 CrossRef Medline
22. Shalem, O., Sanjana, N. E., and Zhang, F. (2015) High-throughput functional genomics using CRISPR–Cas9. *Nature* **16,** 299–311 CrossRef Medline
23. Wang, T., Wei, J. J., Sabatini, D. M., and Lander, E. S. (2014) Genetic screens in human cells using the CRISPR-Cas9 system. *Science* **343,** 80–84 CrossRef Medline
24. Canver, M. C., Smith, E. C., Sher, F., Pinello, L., Sanjana, N. E., Shalem, O., Chen, D. D., Schupp, P. G., Vinjamur, D. S., Garcia, S. P., Luc, S., Kurita, R., Nakamura, Y., Fujiwara, Y., Maeda, T., *et al.* (2015) BCL11A enhancer dissection by Cas9-mediated *in situ* saturating mutagenesis. *Nature* **527,** 192–197 CrossRef Medline
25. Korkmaz, G., Lopes, R., Ugalde, A. P., Nevedomskaya, E., Han, R., Myacheva, K., Zwart, W., Elkon, R., and Agami, R. (2016) Functional genetic screens for enhancer elements in the human genome using CRISPR-Cas9. *Nat. Biotechnol.* **34,** 192–198 CrossRef Medline
26. Rajagopal, N., Srinivasan, S., Kooshesh, K., Guo, Y., Edwards, M. D., Banerjee, B., Syed, T., Emons, B. J. M., Gifford, D. K., and Sherwood, R. I. (2016) High-throughput mapping of regulatory DNA. *Nat. Biotechnol.* **34,** 167–174 CrossRef Medline
27. Diao, Y., Li, B., Meng, Z., Jung, I., Lee, A. Y., Dixon, J., Maliskova, L., Guan, K.-L., Shen, Y., and Ren, B. (2016) A new class of temporarily phenotypic enhancers identified by CRISPR/Cas9-mediated genetic screening. *Genome Res.* **26,** 397–405 CrossRef Medline
28. Diao, Y., Fang, R., Li, B., Meng, Z., Yu, J., Qiu, Y., Lin, K. C., Huang, H., Liu, T., Marina, R. J., Jung, I., Shen, Y., Guan, K.-L., and Ren, B. (2017) A tiling-

deletion-based genetic screen for cis-regulatory element identification in mammalian cells. *Nat. Methods* **14,** 629–635 CrossRef Medline
29. Sanjana, N. E., Wright, J., Zheng, K., Shalem, O., Fontanillas, P., Joung, J., Cheng, C., Regev, A., and Zhang, F. (2016) High-resolution interrogation of functional elements in the noncoding genome. *Science* **353,** 1545–1549 CrossRef Medline
30. Whyte, W. A., Orlando, D. A., Hnisz, D., Abraham, B. J., Lin, C. Y., Kagey, M. H., Rahl, P. B., Lee, T. I., and Young, R. A. (2013) Master transcription factors and mediator establish super-enhancers at key cell identity genes. *Cell* **153,** 307–319 CrossRef Medline
31. Yeom, Y. I., Fuhrmann, G., Ovitt, C. E., Brehm, A., Ohbo, K., Gross, M., Hübner, K., and Schöler, H. R. (1996) Germline regulatory element of Oct-4 specific for the totipotent cycle of embryonal cells. *Development* **122,** 881–894 Medline
32. Seruggia, D., Oti, M., Tripathi, P., Canver, M. C., LeBlanc, L., Di Giammartino, D. C., Bullen, M. J., Nefzger, C. M., Sun, Y. B. Y., Farouni, R., Polo, J. M., Pinello, L., Apostolou, E., Kim, J., Orkin, S. H., *et al.* (2019) TAF5L and TAF6L maintain self-renewal of embryonic stem cells via the MYC regulatory network. *Mol. Cell* **74,** 1148–1163.e7 CrossRef Medline
33. Szabó, P. E., Hübner, K., Schöler, H., and Mann, J. R. (2002) Allele-specific expression of imprinted genes in mouse migratory primordial germ cells. *Mech. Dev.* **115,** 157–160 CrossRef Medline
34. Hsu, P. D., Scott, D. A., Weinstein, J. A., Ran, F. A., Konermann, S., Agarwala, V., Li, Y., Fine, E. J., Wu, X., Shalem, O., Cradick, T. J., Marraffini, L. A., Bao, G., and Zhang, F. (2013) DNA targeting specificity of RNA-guided Cas9 nucleases. *Nat. Biotechnol.* **31,** 827–832 CrossRef Medline
35. Canver, M. C., Lessard, S., Pinello, L., Wu, Y., Ilboudo, Y., Stern, E. N., Needleman, A. J., Galactéros, F., Brugnara, C., Kutlar, A., McKenzie, C., Reid, M., Chen, D. D., Das, P. P., Cole, M. A., *et al.* (2017) Variant-aware saturating mutagenesis using multiple Cas9 nucleases identifies regulatory elements at trait-associated loci. *Nature* **49,** 625–634 CrossRef Medline
36. Murakawa, Y., Yoshihara, M., Kawaji, H., Nishikawa, M., Zayed, H., Suzuki, H., Fantom Consortium, and Hayashizaki, Y. (2016) Enhanced identification of transcriptional enhancers provides mechanistic insights into diseases. *Trends Genet.* **32,** 76–88 CrossRef Medline
37. van de Werken, H. J. G., Landan, G., Holwerda, S. J. B., Hoichman, M., Klous, P., Chachik, R., Splinter, E., Valdes-Quezada, C., Oz, Y., Bouwman, B. A. M., Verstegen, M. J. A. M., de Wit, E., Tanay, A., and de Laat, W. (2012) Robust 4C-seq data analysis to screen for regulatory DNA interactions. *Nat. Methods* **9,** 969–972 CrossRef Medline
38. Hsieh, T.-H. S., Cattoglio, C., Slobodyanyuk, E., Hansen, A. S., Rando, O. J., Tjian, R., and Darzacq, X. (2020) Resolving the 3D landscape of transcription-linked mammalian chromatin folding. *Mol. Cell* **78,** 539–553.e8 CrossRef Medline
39. Long, H. K., Prescott, S. L., and Wysocka, J. (2016) Ever-changing landscapes: transcriptional enhancers in development and evolution. *Cell* **167,** 1170–1187 CrossRef Medline
40. Fulco, C. P., Munschauer, M., Anyoha, R., Munson, G., Grossman, S. R., Perez, E. M., Kane, M., Cleary, B., Lander, E. S., and Engreitz, J. M. (2016) Systematic mapping of functional enhancer-promoter connections with CRISPR interference. *Science* **354,** 769–773 CrossRef Medline
41. Das, P. P., Shao, Z., Beyaz, S., Apostolou, E., Pinello, L., De Los Angeles, A., O'Brien, K., Atsma, J. M., Fujiwara, Y., Nguyen, M., Ljuboja, D., Guo, G., Woo, A., Yuan, G.-C., Onder, T., *et al.* (2014) Distinct and combinatorial functions of Jmjd2b/Kdm4b and Jmjd2c/Kdm4c in mouse embryonic stem cell identity. *Mol. Cell* **53,** 32–48 CrossRef Medline
42. Bolger, A. M., Lohse, M., and Usadel, B. (2014) Trimmomatic: a flexible trimmer for Illumina sequence data. *Bioinformatics* **30,** 2114–2120 CrossRef Medline
43. Langmead, B., and Salzberg, S. L. (2012) Fast gapped-read alignment with Bowtie 2. *Nat. Methods* **9,** 357–359 CrossRef Medline
44. Zhang, Y., Liu, T., Meyer, C. A., Eeckhoute, J., Johnson, D. S., Bernstein, B. E., Nusbaum, C., Myers, R. M., Brown, M., Li, W., and Liu, X. S. (2008) Model-based analysis of ChIP-Seq (MACS). *Genome Biol.* **9,** R137 CrossRef Medline
45. Durand, N. C., Shamim, M. S., Machol, I., Rao, S. S. P., Huntley, M. H., Lander, E. S., and Aiden, E. L. (2016) Juicer provides a one-click system for analyzing loop-resolution Hi-C experiments. *Cell Syst.* **3,** 95–98 CrossRef Medline